



## Obrabotka metallov -

## Metal Working and Material Science

Journal homepage: [http://journals.nstu.ru/obrabotka\\_metallov](http://journals.nstu.ru/obrabotka_metallov)









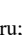
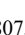
### Effect of heterogeneous structure on mechanical behavior of austenitic stainless steel subjected to novel thermomechanical processing





Ruslan Chernichenko<sup>1, a,\*</sup>, Dmitrii Panov<sup>1, b</sup>, Stanislav Naumov<sup>1, s</sup>, Egor Kudryavtsev<sup>1, d</sup>,  
 Gennady Salishchev<sup>1, e</sup>, Alexey Pertsev<sup>2, f</sup>

<sup>1</sup> Belgorod National Research University, 85 Pobedy Str., Belgorod, 308015, Russian Federation

<sup>2</sup> Department Chief Metallurgist, Perm Scientific-Research Technological Institute, 41 Geroev Khasana Str., Perm, 614990, Russian Federation

<sup>a</sup>  <https://orcid.org/0000-0002-8619-0700>,  [rus.chernichenko@mail.ru](mailto:rus.chernichenko@mail.ru); <sup>b</sup>  <https://orcid.org/0000-0002-8971-1268>,  [dimmak-panov@mail.ru](mailto:dimmak-panov@mail.ru);

<sup>c</sup>  <https://orcid.org/0000-0002-4084-8861>,  [NaumovStanislav@yandex.ru](mailto:NaumovStanislav@yandex.ru); <sup>d</sup>  <https://orcid.org/0000-0003-1113-0807>,  [kudryavtsev@bsuedu.ru](mailto:kudryavtsev@bsuedu.ru);

<sup>e</sup>  <https://orcid.org/0000-0002-0815-3525>,  [salishchev\\_g@bsuedu.ru](mailto:salishchev_g@bsuedu.ru); <sup>f</sup>  <https://orcid.org/0009-0009-0771-9345>,  [perets\\_87@mail.ru](mailto:perets_87@mail.ru)

#### ARTICLE INFO

##### Article history:

Received: 17 February 2025

Revised: 05 March 2025

Accepted: 21 March 2025

Available online: 15 June 2025

##### Keywords:

Austenitic stainless steel

Heterogeneous structure

Axial texture

Shear texture

Cold radial forging

Heat treatment

Strength

Ductility

##### Funding

This work was supported by the Russian Science Foundation (Agreement No. 20-79-10094) using the equipment of BSU Shared Research Facilities "Technologies and Materials".

#### ABSTRACT

**Introduction.** The low yield strength of austenitic stainless steels is a factor significantly limiting their industrial applications. In turn, the formation of a heterogeneous structure is a promising method for achieving a synergy of mechanical properties. At the same time, an effective way to obtain a bulk heterogeneous structure is cold radial forging. However, the underlying mechanisms for the improved mechanical properties of materials with a heterogeneous structure formed in the process of cold radial forging are currently poorly understood. **Purpose of the work** is to investigate the effect of a heterogeneous structure obtained by deformation and heat treatment on the mechanical properties of austenitic stainless steel *0.08 C-17 Cr-13 Ni-2 Mn-Ti*. **Methods.** Uniaxial tensile tests were performed on specimens obtained by cold radial forging followed by heat treatment at 600–700°C, using an *Instron 5882* testing machine at room temperature with a strain rate of  $1.15 \times 10^{-3} \text{ s}^{-1}$ . A *VIC-3D* visual inspection system was used to measure elongation during testing. The fine structure was examined on perforated foils with a diameter of 3 mm using a *JEOL JEM-2100* transmission electron microscope at an accelerating voltage of 200 kV. **Results and discussion.** It was shown that, after thermo-mechanical treatment, a twin-matrix austenite structure was obtained in the center of the rod, while an ultrafine-grained structure with isolated recrystallized austenite grains of approximately 1 μm in size was obtained at the edge. It was established that a two-component axial austenite texture  $\langle 001 \rangle / \langle 111 \rangle$  is formed in the center of the rod, which transformed into a shear texture  $B/\bar{B}$  towards the rod surface. It was determined that the formation of a heterogeneous structure led to additional strengthening due to back stresses. It was found that, after heat treatment at 700 °C, the specimen with a heterogeneous structure exhibited the highest yield strength, equal to 1054 MPa, with a relative elongation of 16%. Thus, the employed thermo-mechanical treatment may be a promising method for obtaining large-sized rod stocks from austenitic stainless steel *0.08 C-17 Cr-13 Ni-2 Mn-Ti* with high mechanical properties.

**For citation:** Chernichenko R.S., Panov D.O., Naumov S.V., Kudryavtsev E.A., Salishchev G.A., Pertsev A.S. Effect of heterogeneous structure on mechanical behavior of austenitic stainless steel subjected to novel thermomechanical processing. *Obrabotka metallov (tekhnologiya, oborudovanie, instrumenty)* = *Metal Working and Material Science*, 2025, vol. 27, no. 2, pp. 189–205. DOI: 10.17212/1994-6309-2025-27.2-189-205. (In Russian).

## Introduction

Austenitic stainless steels are a unique class of materials that combine high mechanical, physical, and chemical properties, making them a widely used structural material [1, 2]. However, a major disadvantage that limits the scope of application of these steels is their reduced strength characteristics [3]. Traditional

#### \* Corresponding author

Chernichenko Ruslan S., Research assistant

Belgorod National Research University,

85 Pobedy Str.,

308015, Belgorod, Russian Federation

Tel.: +7 905 172-05-92, e-mail: [rus.chernichenko@mail.ru](mailto:rus.chernichenko@mail.ru)

strategies for increasing strength characteristics often lead to a significant decrease in impact strength and ductility [4–6]. For example, processing an *AISI 304* austenitic stainless steel by cold rolling can increase the yield strength by more than twofold (from 640 MPa to 1,450 MPa). At the same time, a critical decrease in elongation to failure to 1 % is observed [7]. In this case, the change in mechanical properties is caused not only by strain hardening but also by the formation of deformation-induced martensite ( $\alpha'$ ). According to Ref. [6], deformation-induced martensite ( $\alpha'/\epsilon$ ) can act as a site for crack nucleation because it is a brittle product of phase transformation, which also causes a decrease in impact toughness and ductility, simultaneously with an increase in strength characteristics [8]. In this case, the crack can propagate both within the martensite itself and along the interface between the deformation-induced martensite and the austenitic matrix [9].

In recent years, it has been shown that increasing strength properties without loss of ductility in austenitic steels is possible through the formation of heterogeneous structures [9–15]. A heterogeneous condition is understood as a structure that consists of structural elements of different sizes or chemical composition, which significantly impacts the mechanical properties of the material [16]. Such structures include heterogeneous lamellar structures [17], gradient structures [18], bimodal structures, etc. Thus, it is shown [17] that titanium samples with a heterogeneous lamellar structure formed during asymmetric rolling and subsequent recrystallization annealing exhibit strength at the level of samples with an ultrafine-grained (*UFG*) structure and ductility comparable to a material with a coarse-grained structure. *AISI 304* steel samples with a gradient structure consisting of a central layer with microtwins and nanotwins in the subsurface layers have a yield strength of 820 MPa and a uniform elongation of 53 % [18]. In contrast, samples of such steel with a homogeneous structure demonstrate a yield strength of 268 MPa and a uniform elongation of 63 %.

The literature reports on the production of heterogeneous structures in rod blanks using cold radial forging (*CRF*) [10, 19–22]. It has been shown that the *CRF* of rods made of *AISI 316Ti* steel to a 95 % area reduction leads to the formation of a heterogeneous structure in the cross-section. Notably, increasing the area reduction from 40 % to 80 % positively affects the material's strength characteristics. Specifically, a 15 % increase in yield strength is observed, while ductility remains at the same level. Furthermore, low-temperature heat treatment at 400–600°C of the *CRF* rod causes a significant increase in the yield strength (from 1,077 to 1,310 MPa) [22]. Along with this, an increase in the elongation to failure from 9 % to 11 % is observed. It is important to note that structural heterogeneity is preserved after low-temperature heat treatment. Despite the existing research on the formation of heterogeneous structures during *CRF*, the underlying mechanisms responsible for improving mechanical properties through heterostructuring treatment remain unclear.

**The purpose of this work** is to study the effect of heterogeneity obtained during *CRF* and subsequent heat treatment on the mechanical properties of *0.08 C-17 Cr-13 Ni-2 Mn-Ti* austenitic stainless steel. **To achieve this purpose, the following tasks were set during the study:**

- to study the effect of thermomechanical processing on the formation of heterogeneous structure and texture in the rod;
- to study the effect of the heterogeneous structure obtained during thermomechanical processing on the mechanical properties of the material under study.

## Methods

*0.08 C-17 Cr-13 Ni-2 Mn-Ti* austenitic stainless steel was selected as the subject of research in the present study. The chemical composition of the studied steel included the following elements (wt. %): 0.08% C, 16.4% Cr, 12.3% Ni, 2.18% Mo, 1.28% Mn, 0.42% Si, 0.2% Ti, with Fe as the balance.

The original rod was obtained by *CRF* to a 95 % area reduction using a forging machine with radially moving dies. *CRF* was carried out using the following parameters: a strike frequency of 1,000 strikes per minute, a feed speed of 180 millimeters per minute, and a rotation speed of 25 rotations per minute. To prevent overheating of the workpiece during *CRF*, the rod was cooled by an external water supply. The state

of the rod after *CRF* to a 95 % area reduction was taken as the initial state. Then, the cold-forged rod was subjected to heat treatment at temperatures of 600 °C (95 % *CRF* + *HT* 600 °C) and 700 °C (95 % *CRF* + *HT* 700 °C) followed by air cooling. The holding time was 2 hours.

For microstructure characterization, steel disks with a diameter of 3 mm, mechanically thinned to 100–150 µm and electrolytically perforated, were examined using a *JEOL JEM-2100* transmission electron microscope (*TEM*) with an accelerating voltage of 200 kV. To confirm structural heterogeneity, blanks for *TEM* studies were cut in the cross-section from the center and edge of the studied steel rod. Perforation was performed on a *TenuPol-5* setup using an electrolyte consisting of 10 % perchloric acid and 90 % acetic acid.

Uniaxial tensile tests of steel specimens were carried out at room temperature using an *Instron 5882* testing machine at a strain rate of  $1.15 \times 10^{-3} \text{ s}^{-1}$ . For a more accurate determination of the deformation degree, the *VIC-3D* visual inspection system was used. Subsequent processing of the obtained data was carried out using *VIC-2D* software. To determine the mechanical properties of different regions, specimens were cut from the center (*sample C* – center) and edge (*sample E* – edge) of the rod. To determine the mechanical properties of a specimen with a heterogeneous structure, flat specimens were cut along the entire diameter of the rod (*sample H* – with a heterogeneous structure), with a width corresponding to the diameter of the rod. The cutting diagram is shown in Fig. 1. The gauge length of the steel tensile specimens was calculated according to *GOST 1497–23*:

$$l_0 = 5.65\sqrt{F_0}, \quad (1)$$

where  $l_0$  is the gauge length of the specimen;  $F_0$  is the cross-sectional area.

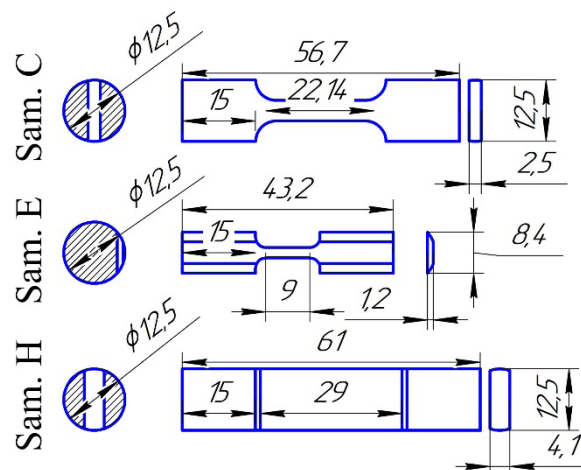


Fig. 1. Uniaxial tensile specimen cutting scheme and dimensions (mm) for:

central rod portion (*C* – center), subsurface layer (*E* – edge), and the entire structural zone (*H* – heterogeneous)

For identification of samples in the case of subsequent heat treatment, a number denoting the annealing temperature is added to the corresponding letter, defining the area of samples cutting (e.g., *E600* is a sample cut from the rod edge subjected to heat treatment at 600 °C). For a deformed sample, the number 95 is added, denoting the area reduction (e.g., *E95* is a sample cut from the edge of a rod subjected to *CRF*).

To determine the magnitude of back stresses in each region, load-unload tests were carried out on the corresponding samples under conditions of uniform plastic deformation at  $\varepsilon = 2\text{--}5\%$ . Calculations were performed according to the methodology presented in Refs. [17, 23]. The samples were tested in the state after *CRF* to 95 % followed by heat treatment at 700 °C for 2 hours. During the tests, stress-strain curves with hysteresis loops were obtained (Fig. 2). The level of back stresses was determined by the following equation [17, 23]:

$$\sigma_b = \frac{\sigma_r + \sigma_u}{2}, \quad (2)$$

where  $\sigma_b$  are the back stresses (MPa);  $\sigma_r$  are the flow stresses under repeated loading (MPa);  $\sigma_u$  are the flow stresses under unloading (MPa).

Flow stresses under repeated loading and unloading were determined from the hysteresis loops according to the scheme shown in Fig. 2.

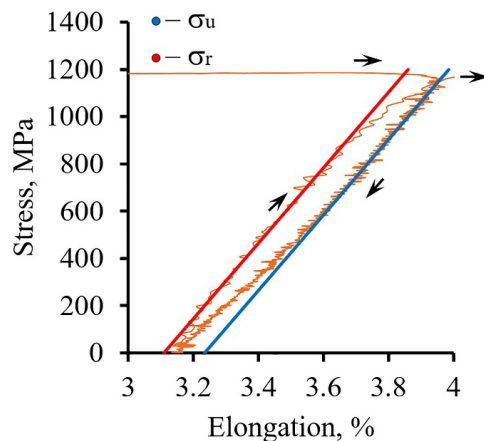


Fig. 2. Schematic showing the method for determining the yield stress at unloading ( $\sigma_u$ ) and the stress at reloading ( $\sigma_r$ )

## Results and discussion

The microstructure of the rod center (Fig. 3, *a*), subjected to 95 % CRF, consists of parallelogram-shaped domains (marked with a yellow dotted line), formed by mechanical twins of various systems. Dislocation cells can be observed inside such structural elements (marked with a green dotted line). In turn, the structure of the subsurface layer (Fig. 3, *b*) is ultrafine-grained (UFG). In this case, the size of the structural elements of the central part ( $700 \pm 490$  nm) (Fig. 3, *a*) significantly exceeds the sizes of the elements forming the structure of the subsurface layer ( $100 \pm 50$  nm) (Fig. 3, *b*).

Following heat treatment at 600 °C, polygonization is activated over the entire cross section of the rod, which causes additional refinement of the structure due to the formation of dislocation walls (Fig. 4, *a* and 4, *b*). Heat treatment at 700 °C is accompanied by the formation of recrystallization nuclei in highly deformed subsurface layers (Fig. 4, *d*) and the continuation of dislocation redistribution processes in the rod center. As a result, areas with a reduced dislocation density - “dislocation-free” regions - are

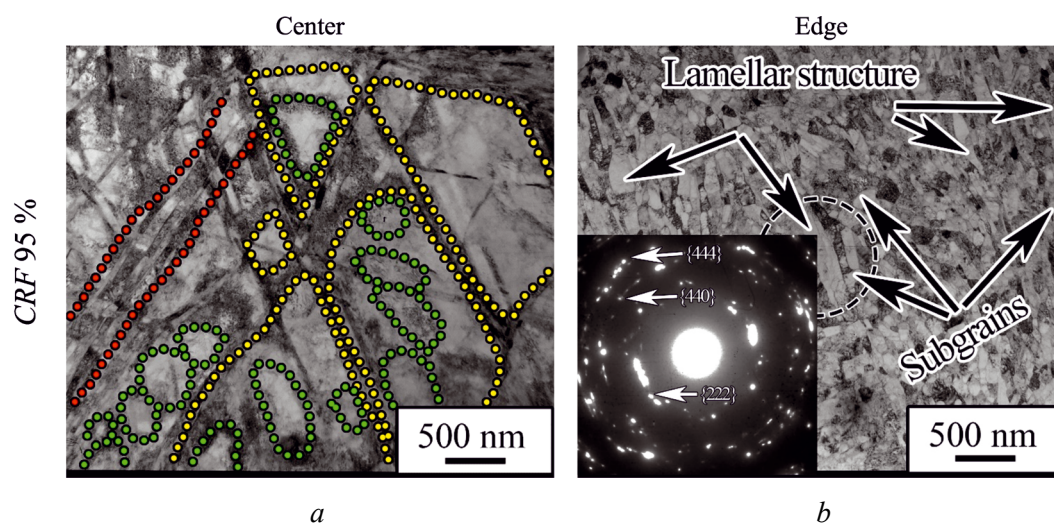


Fig. 3. Fine structure of the center (*a*) and subsurface layer (*b*) of a steel rod subjected to 95% CRF



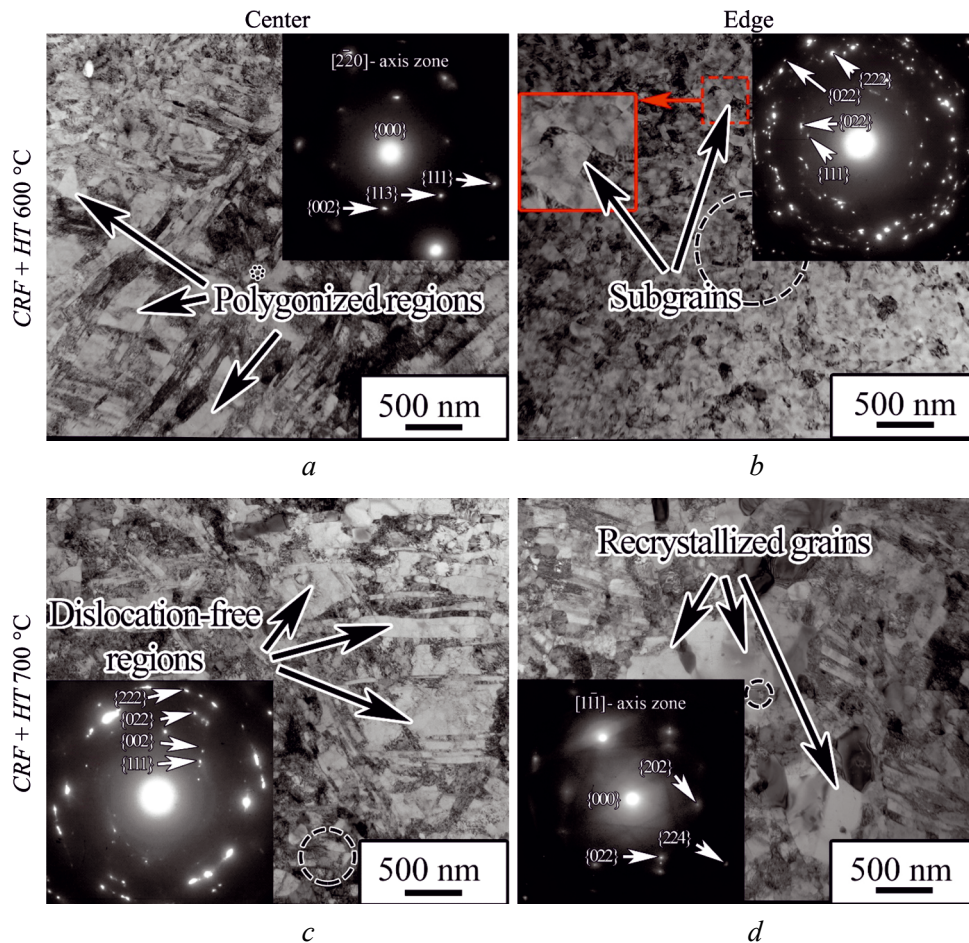


Fig. 4. Fine structure of the center (a, c) and subsurface layer (b, d) of a steel rod subjected to annealing at 600 °C (a, b) and 700 °C (c, d)

formed in the rod center (Fig. 4, c). However, the heterogeneous structure obtained during *CRF* has high thermal stability. The evolution of the microstructure during *CRF* and subsequent annealing is considered in more detail in earlier works [21, 22].

Fig. 5 shows the *Kikuchi* line contrast maps (Fig. 5,  $a_1$ – $a_2$ ), kernel average misorientation (*KAM*) maps (Fig. 5,  $b_1$ – $b_2$ ), crystal direction maps (Fig. 5,  $c_1$ – $c_2$ ), direct (Fig. 5,  $d_1$ – $d_2$ ) and inverse (Fig. 5,  $e_1$ – $e_2$ ) pole figures of the material under study after the thermomechanical treatment. It is worth noting that for the center of the rod, the *Kikuchi* line contrast maps (Fig. 5,  $a_1$ ) and *KAM* maps (Fig. 5,  $b_1$ ) are of higher quality. 95 % *CRF* leads to the high *KAM* value both in the center and at the edge of the rod (Fig. 5,  $b_1$ – $b_2$ ). Moreover, in the subsurface layer (Fig. 5,  $b_2$ ), the *KAM* value is higher than that in the rod center (Fig. 5,  $b_1$ ). In addition, the pronounced two-component axial texture  $\langle 001 \rangle / \langle 111 \rangle$  is formed in the rod center (Fig. 5,  $c_1$ ,  $d_1$ ). However, the subsurface layer is characterized by the shear texture  $B/B^-$  (Fig. 5,  $d_2$ ) [24–26]. In addition, according to the crystal direction maps (Fig. 5,  $c_1$ – $c_2$ ), a decrease in the volume fraction of grains of both orientations is observed in the cross section of the rod in the direction from the center to the edge. Namely, from the center to the subsurface layer, the fraction of  $\langle 001 \rangle$ -oriented grains decreases from 38 % to 5 %, with a decrease in the fraction of grains with the  $\langle 111 \rangle$ -orientation from 50 % to 30 %.

Subsequent heat treatment at 600–700 °C improves the quality of the *Kikuchi* line contrast maps (Fig. 6,  $a_1$ – $a_4$ ) and *KAM* maps (Fig. 6,  $b_1$ – $b_4$ ) for all areas. However, of *KAM* value remains high throughout the rod cross section with a characteristic increase in the direction from the center to the edge (Fig. 6,  $b_1$ – $b_4$ ). Obviously, the highest *KAM* value is recorded along the grain boundaries and mechanical twins, while in the body of the grains this indicator is minimal (Fig. 6,  $b_1$ – $b_4$ ). In addition, in the subsurface layer, the formation of new small areas with the low *KAM* value is observed (Fig. 6,  $a_4$  and  $a_4$ , indicated by white arrows). In the rod center, the two-component axial texture  $\langle 001 \rangle / \langle 111 \rangle$  is preserved



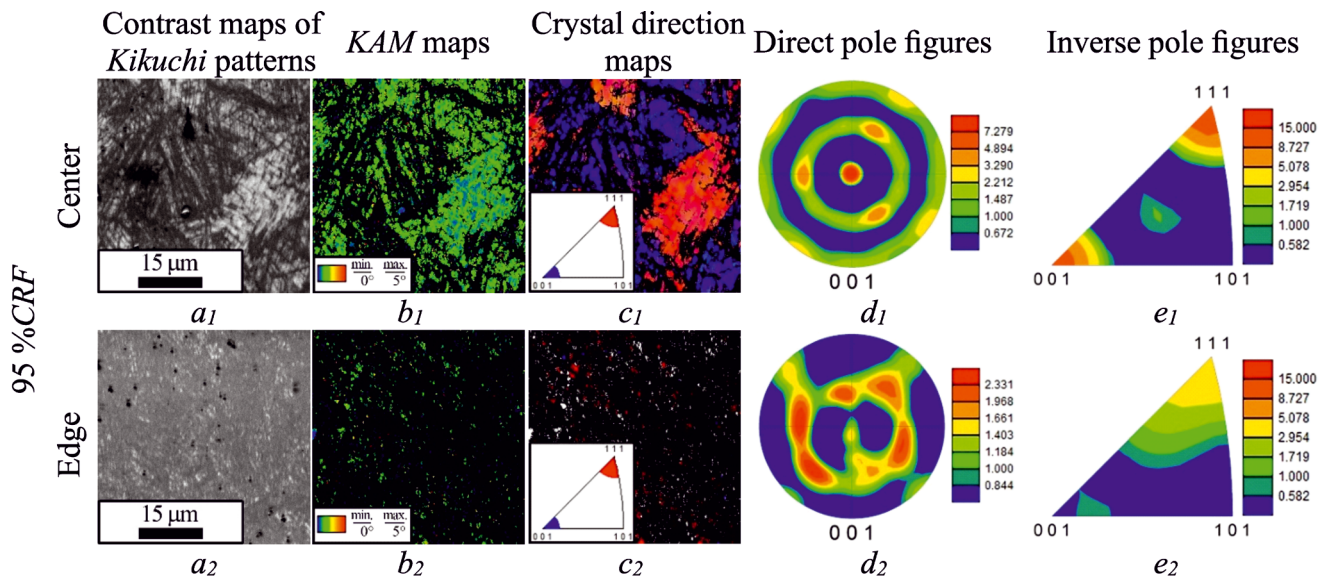


Fig. 5. Kikuchi line contrast maps ( $a_1$ - $a_2$ ), KAM maps ( $b_1$ - $b_2$ ), crystal direction maps ( $c_1$ - $c_2$ ), direct ( $d_1$ - $d_2$ ) and inverse ( $e_1$ - $e_2$ ) pole figures of the steel rod subjected to 95% CRF

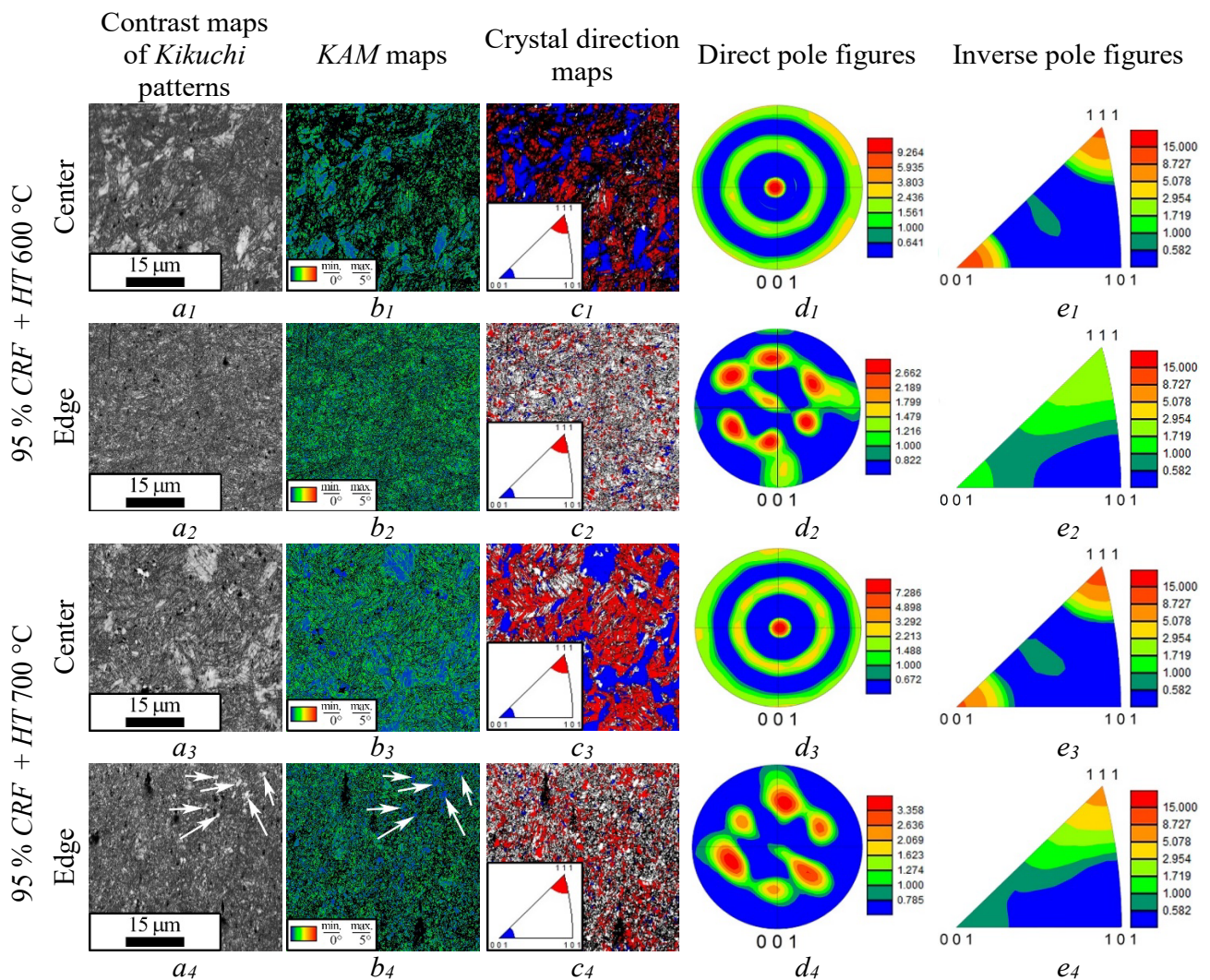


Fig. 6. Kikuchi line contrast maps ( $a_1$ - $a_4$ ), KAM maps ( $b_1$ - $b_4$ ), crystal direction maps ( $c_1$ - $c_4$ ), direct ( $d_1$ - $d_4$ ) and inverse ( $e_1$ - $e_4$ ) pole figures of the steel rod subjected to annealing at 600 °C ( $a_1$ - $a_2$ ,  $b_1$ - $b_2$ ,  $c_1$ - $c_2$ ,  $d_1$ - $d_2$ ,  $e_1$ - $e_2$ ) and 700 °C ( $a_3$ - $a_4$ ,  $b_3$ - $b_4$ ,  $c_3$ - $c_4$ ,  $d_3$ - $d_4$ ,  $e_3$ - $e_4$ )

(Fig. 6,  $d_1$ ,  $d_3$ ), whereas, in the subsurface layer, the shear texture  $B/B^-$  is detected (Fig. 6,  $d_2$ ,  $d_4$ ). In the direction from the center to the edge, the volume fraction of grains with the  $\langle 001 \rangle$ -orientation decreases from 37 % to 4.4 %, and the fraction of grains with the  $\langle 111 \rangle$ -orientation decreases from 48 % to 31 % (Fig. 6,  $c_1$ - $c_4$ ).

Analysis of the obtained results showed that a pronounced heterogeneous structure is formed in the cross-section of the rod during the applied thermomechanical treatment. The phenomenon is associated with the non-uniform stress state of the rod during *CRF* [21]. Specifically, moderate tensile stress acts in the rod center and high compressive stress operates in the subsurface layers. The non-uniform stress state leads to the activation of various plastic deformation mechanisms in the center and subsurface layers of the rod. Mechanical twinning and dislocation slip are observed in the center of the rod, developing large structural elements in the form of regions with dislocation cells limited by packages of mechanical twins. In this case, according to Ref. [25], twinned microvolumes have the  $\langle 111 \rangle$ -orientation, and microvolumes with a cellular structure have the  $\langle 100 \rangle$ -orientation, which ultimately leads to the formation of the axial two-component texture  $\langle 001 \rangle / \langle 111 \rangle$  in the rod center.

On the other hand, high compressive stresses in the subsurface layer contribute to the formation of shear bands, since the possibilities for deformation accommodation due to dislocation sliding and mechanical twinning are quickly exhausted during *CRF*. At the same time, shear bands were found after *CRF* with a degree of 60 % [21]. The formation of shear bands leads to the formation of a UFG structure via the rotational recrystallization mechanism, which was proposed by *V.F. Nesterenko et al.* [27]. In essence, during the deformation process, a shear band is enhanced, within which there are randomly distributed dislocations that form elongated dislocation cells. The latter transform into subgrains with an increase in accumulated plastic strain. During further deformation, these subgrains are fragmented with the subsequent formation of equiaxed micrograins. In addition, the change in the predominant mechanism of plastic deformation explains a decrease in the proportion of grains with  $\langle 100 \rangle$ - and  $\langle 111 \rangle$ -orientations in the direction from the edge to the center. It should be noted that the shear texture  $B/B^-$  in the subsurface layer is caused by shear banding.

Heat treatment at 600 °C does not have a significant effect on the microstructure and texture of the rod. However, partial polygonization occurs throughout the entire cross-section. After heat treatment at 700 °C, recrystallization nuclei were found in the subsurface layer, the fraction of which in the microstructure is less than 10 %.

Tensile stress-strain curves (Fig. 7) were obtained for samples of different types (Fig. 1). After 95 % *CRF* for all types of samples (*Samples C, E and H*) the stress-strain curve is typical for cold-deformed steels with high strength and low ductility (Fig. 7,  $a_1$ ). When the yield strength is reached, a peak is observed on the curve, followed by a region of strain localization. Heat treatment at 600 °C does not have a significant effect on the shape of the stress-strain curves of the *E600* and *H600* samples, but an increase in strength characteristics is observed (Fig. 7,  $b_1$ ). In this case, the sample *C600* shows an increase in the uniform deformation area and a decrease in strength characteristics. In turn, after heat treatment at 700 °C, the curves in all cases demonstrate a lower level of strength characteristics and an increase in ductility (Fig. 7,  $c_1$ ).

Based on the curves of strain hardening rate, it is evident that for all three types of samples after 95 % *CRF*, only one stage of strain hardening is observed, which is limited by the onset of strain localization (Fig. 7,  $a_{2-4}$ ). In turn, heat treatment at 600 °C did not significantly affect the nature of the curve of samples *E600* (Fig. 7,  $b_3$ ) and *H600* (Fig. 7,  $b_4$ ). While on the curve obtained for the sample *C600* (Fig. 7,  $b_2$ ), three stages of strain hardening can be distinguished. At the first stage, a sharp decrease in strain hardening occurs. The beginning of the second stage is characterized by a change in the slope of the curve, stabilization and an increase in strain hardening rate. Apparently, a decrease in the strain-hardening rate is related to the activation of dynamic recovery.

The stage-by-stage nature of the strain-hardening behavior are described in detail in Ref. [28]. Namely, the first stage of strain hardening can be associated with the redistribution and annihilation of dislocations, which causes a decrease in the strain-hardening rate. With an increase in true strain, the second stage begins, which is associated with mechanical twinning. Therefore, the strain-hardening rate increases or sta-

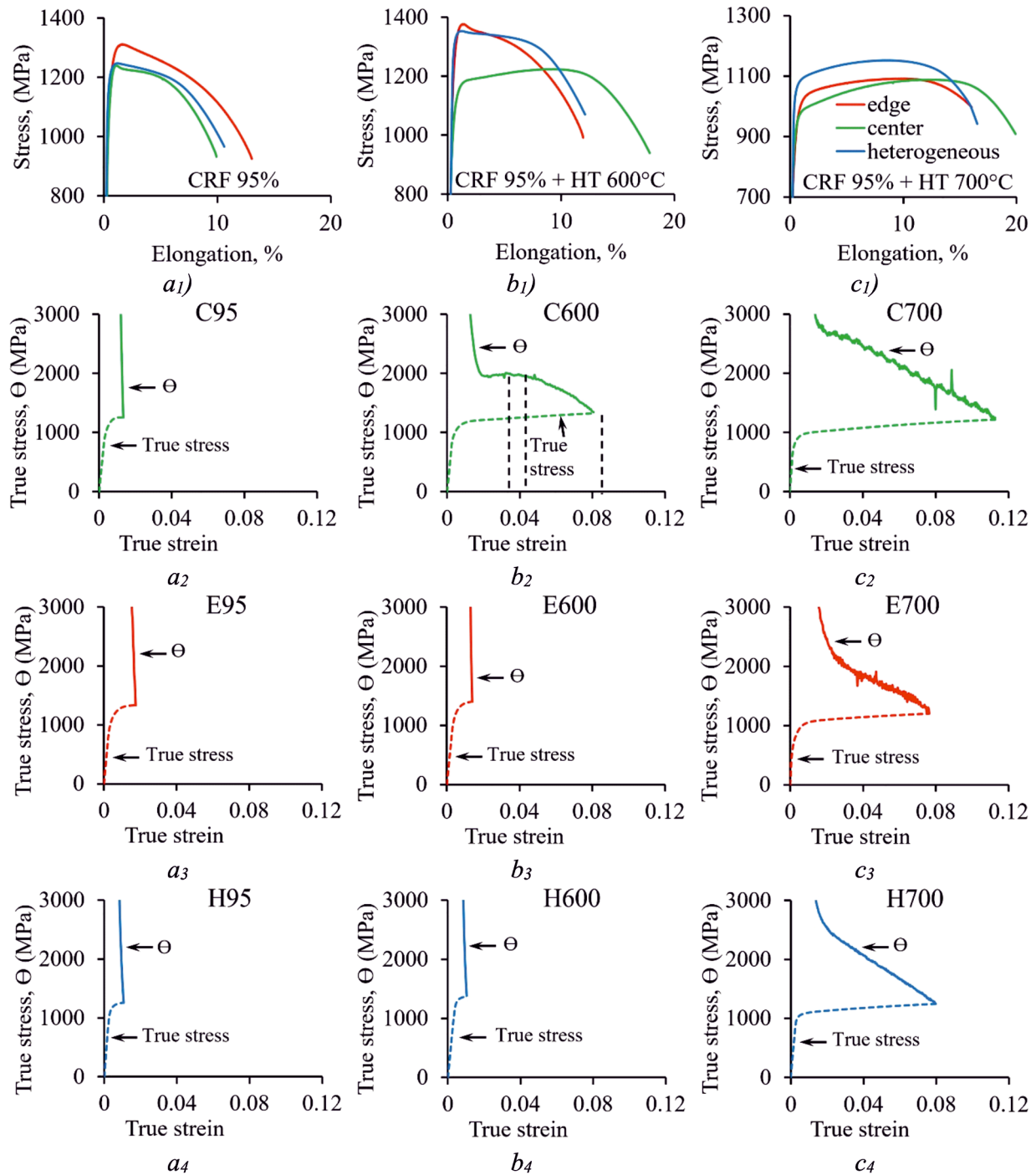


Fig. 7. Stress-strain curves ( $a_1$ ,  $b_1$ ,  $c_1$ ) and work hardening behavior of the center ( $a_2$ ,  $b_2$ ,  $c_2$ ), edge ( $a_3$ ,  $b_3$ ,  $c_3$ ) and heterogeneous ( $a_4$ ,  $b_4$ ,  $c_4$ ) material after different modes of thermo-mechanical treatment

bilizes. Due to the saturation of mechanical twinning, the strain hardening rate decreases at the third stage (Fig. 7,  $b_2$ ).

In the present study, the stage-like strain hardening is ascribed to the heterogeneous microstructure (Fig. 7). On the curves for all three types of samples obtained from a rod after heat treatment at 700 °C, two stages of strain hardening can be distinguished (Fig. 7,  $b_{2-4}$ ). The first stage is also characterized by a sharp decrease in strain hardening. At the second stage, the slope of the curve changes, and the decrease in strain hardening rate becomes less intense.

Table presents that all three types of samples after 95 % CRF have high strength and low ductility. The ultimate tensile strength ( $\sigma_u$ ) is 1,240-1,300 MPa, and the yield strength ( $\sigma_{0.2}$ ) is 1,150-1,210 MPa.



### Mechanical properties characteristics

Region	Heterogeneous ( <i>H</i> )	Centre ( <i>C</i> )	Edge ( <i>E</i> )
95% <i>CRF</i>			
$\sigma_u$ (MPa)	$1,242 \pm 7$	$1,259 \pm 28$	$1,303 \pm 13$
$\sigma_{0.2}$ (MPa)	$1,210 \pm 11$	$1,147 \pm 100$	$1,197 \pm 1$
$\delta$ (%)	$8.3 \pm 1.2$	$8.4 \pm 1.4$	$11.5 \pm 0.9$
$\delta_u$ (%)	$1 \pm 0.1$	$0.7 \pm 0.2$	$1.1 \pm 0.1$
95% <i>CRF</i> + <i>HT</i> 600°C for 2 hours			
$\sigma_u$ (MPa)	$1,355 \pm 2$	$1,225 \pm 35$	$1,374 \pm 3$
$\sigma_{0.2}$ (MPa)	$1,330 \pm 8$	$1,060 \pm 30$	$1,252 \pm 23$
$\delta$ (%)	$10.3 \pm 0.5$	$16.1 \pm 0.5$	$11 \pm 0.3$
$\delta_u$ (%)	$0.8 \pm 0.1$	$9 \pm 0.3$	$1 \pm 0.1$
95% <i>CRF</i> + <i>HT</i> 700°C for 2 hours			
$\sigma_u$ (MPa)	$1,145 \pm 11$	$1,091 \pm 4$	$1,102 \pm 13$
$\sigma_{0.2}$ (MPa)	$1,054 \pm 14$	$927 \pm 15$	$877 \pm 9.2$
$\delta$ (%)	$16 \pm 2.7$	$18.5 \pm 0.8$	$16 \pm 1.3$
$\delta_u$ (%)	$8.1 \pm 0.1$	$11.6 \pm 0.5$	$8.8 \pm 1.3$

Meanwhile, the elongation to failure ( $\delta$ ) is in the range of 8-12 %, while the uniform elongation ( $\delta_u$ ) does not exceed 1 %. After heat treatment at 600 °C, an increase in  $\sigma_u$  and  $\sigma_{0.2}$  of the *E600* and *H600* samples to 1,360-1,370 MPa and 1,250-1,330 MPa, respectively, is observed, but ductility does not change (Table). However, the strength characteristics of the *C600* sample decrease after heat treatment at 600 °C. Namely,  $\sigma_u$  is 1,225 MPa, and  $\sigma_{0.2}$  is 1,060 MPa. Along with this,  $\sigma$  increases to 16 %, and  $\sigma_u$  increases to 9 % (Table). Heat treatment at 700 °C provokes a decrease in strength and an increase in ductility. In particular, the *H700* sample possesses the attractive strength-ductility combination ( $\sigma_u = 1,145$  MPa;  $\sigma_{0.2} = 1,054$  MPa;  $\delta = 16$  %;  $\delta_u = 8$  %).

The heterogeneous structure and texture in the cross section of the rod affect the mechanical behavior of the material under study. High strength characteristics and low ductility of the material after *CRF* are associated with a highly deformed structure. However, the material with the *UFG* structure (from the subsurface layer) exhibits somewhat greater strength and ductility (Fig. 5, *a<sub>1</sub>*). The increased strength of this region is attributed to the *Hall-Petch* strengthening [29, 30], while an increase in ductility is caused by the new grain nucleation [21].

It is worth noting that the pronounced effect of structural and textural heterogeneity on mechanical properties under tension is attained after heat treatment. After heat treatment at 600 °C, the strength of the heterogeneous material increases, while elongation to failure is of 10-11%. On the one hand, an increase in strength characteristics is likely due to the formation of segregations of alloying elements on dislocations [31]. On the other hand, the preservation of ductility is associated with the partial polygonization (Fig. 4, *a*).

Heat treatment at 700 °C, in turn, leads to further softening and an increase in ductility due to the development of polygonization in the center of the rod and the onset of static recrystallization in the subsurface layer. The latter is due to greater accumulated plastic deformation and thereby lower thermal stability [32]. It should be noted that the heterogeneous material after heat treatment at 600-700 °C demonstrates the highest yield strength and good ductility.

According to Ref. [33], a similar effect is ascribed to the increased value of back stresses. Structural heterogeneity is associated with strain partitioning during tensile testing [34]. So, in the strong subsurface

layer, strain localization occurs at the initial stages of plastic strain, but the more ductile rod core prevents further strain localization in subsurface layers, which changes the stress distribution. Such deformation behavior causes the generation and accumulation of geometrically necessary dislocations (*GND*) at the boundary of layers with different structures. In turn, *GND* interact with mobile dislocations and fix them in this area, which provokes additional strain strengthening. In addition, such a stress condition can be accompanied by the activation of additional slip systems [35].

Based on the results of load-unload tests, it is shown that the material with a heterogeneous structure exhibits the highest value of back stresses (Fig. 8). The difference in the value of back stresses is comparable to the difference in the yield strength (Table).

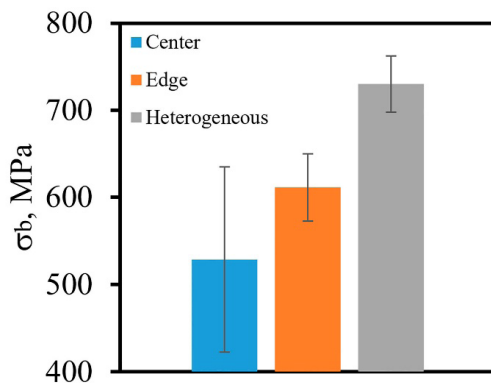
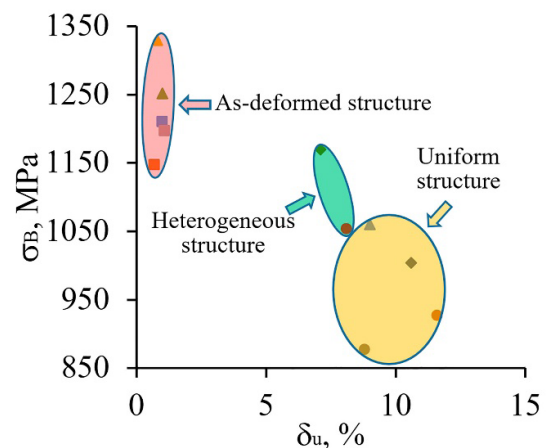


Fig. 8. Back stress levels obtained for specimens with different microstructures, subjected to 95 % CRF, followed by annealing at 700 °C

Thus, based on the results of mechanical tests as a function of the temperature of post-deformation heat treatment for the steel under study, three areas can be distinguished with different strength and ductility ratios, which is graphically shown in Fig. 9. It is obvious that changing the structure type significantly affects mechanical properties. Specifically, the material with a cold-deformed structure is characterized by high strength and low ductility. Steel with a homogeneous structure obtained during post-deformation heat treatment has high ductility and low strength. Whereas, the material with a heterogeneous structure possesses a good balance between strength and ductility.

Fig. 9. Relationship between yield strength ( $\sigma_{0.2}$ ) and proportional elongation ( $\delta_u$ ) of the steel under study in various microstructural conditions



## Conclusion

The effect of a heterogeneous structure obtained during to a 95 % area reduction and subsequent heat treatment at 600-700 °C on mechanical properties of the *AISI 316Ti* steel was studied. The following conclusions are drawn:

1. The proposed thermomechanical treatment forms a heterogeneous structure in the studied steel. The microstructure of the cold-deformed workpiece is changed from a twin-matrix structure in the rod center to a *UFG* structure in the subsurface layer. Heat treatment at 600-700 °C is accompanied by polygonization over the cross section of the rod. Additionally, heat treatment at 700 °C activates the formation of recrystallization nuclei in the subsurface layer. Furthermore, from the center to the edge of the rod, texture



changes from the axial two-component texture  $\langle 001 \rangle / \langle 111 \rangle$  in the rod center to the shear texture  $B/B$  in the subsurface layer.

2. Heterostructured material (annealed at 700 °C) exhibits an enhanced strength-ductility combination ( $\sigma_u = 1,145$  MPa;  $\sigma_{0.2} = 1,054$  MPa;  $\delta = 16$  %;  $\delta_u = 8$  %) compared to the material of the center and edge of the rod. Conversely, heat treatment at 600 °C results in high strength and low ductility ( $\sigma_u = 1,355$  MPa;  $\sigma_{0.2} = 1,330$  MPa;  $\delta = 10.3$  %;  $\delta_u = 0.8$  %), while heat treatment at 800 °C causes pronounced softening and an increase in ductility, which does not allow achieving a good balance of mechanical properties.

## References

1. Lo K.H., Shek C.H., Lai J.K.L. Recent developments in stainless steels. *Materials Science and Engineering: R: Reports*, 2009, vol. 65 (4–6), pp. 39–104. DOI: 10.1016/j.mser.2009.03.001.
2. Kaladhar M., Venkata Subbaiah K., Srinivasa Rao C.H. Machining of austenitic stainless steels – a review. *International Journal of Machining and Machinability of Materials*, 2012, vol. 12 (1–2), pp. 178–192. DOI: 10.1504/IJMMM.2012.048564.
3. Karjalainen L.P., Taulavuori T., Sellman M., Kyröläinen A. Some strengthening methods for austenitic stainless steels. *Steel Research International*, 2008, vol. 79 (6), pp. 404–412. DOI: 10.1002/srin.200806146.
4. Huang J., Ye X., Xu Z. Effect of cold rolling on microstructure and mechanical properties of AISI 301LN metastable austenitic stainless steels. *Journal of Iron and Steel Research International*, 2012, vol. 19 (10), pp. 59–63. DOI: 10.1016/S1006-706X(12)60153-8.
5. Liu Z., Han Y., Wu Z., Sun J., Zu G., Zhu W., Ran X. Microstructures and mechanical properties of cold-rolled 21Cr lean duplex stainless steel with medium to high cold rolling reductions. *Materials Today Communications*, 2022, vol. 33, p. 104860. DOI: 10.1016/j.mtcomm.2022.104860.
6. Huang M., Wang C., Wang L., Wang J., Mogucheva A., Xu W. Influence of DMT on impact toughness: relationship between crack propagation and the  $\alpha'$ -martensite morphology in austenitic steel. *Materials Science and Engineering: A*, 2022, vol. 844, p. 143191. DOI: 10.1016/j.msea.2022.143191.
7. Ozgowicz W., Kurc A. The effect of the cold rolling on the structure and mechanical properties in austenitic stainless steels type 18-8. *Archives of Materials Science and Engineering*, 2009, vol. 38 (1), pp. 26–33.
8. Hwang B., Lee T.H., Park S.J., Oh C.S., Kim S.J. Correlation of austenite stability and ductile-to-brittle transition behavior of high-nitrogen 18Cr-10Mn austenitic steels. *Materials Science and Engineering: A*, 2011, vol. 528 (24), pp. 7257–7266. DOI: 10.1016/j.msea.2011.06.025.
9. Kelly P.M., Rose L.R.F. The martensitic transformation in ceramics – its role in transformation toughening. *Progress in Materials Science*, 2002, vol. 47 (5), pp. 463–557. DOI: 10.1016/S0079-6425(00)00005-0.
10. Panov D.O., Chernichenko R.S., Naumov S.V., Pertsev A.S., Stepanov N.D., Zharebtsov S.V., Salishchev G.A. Excellent strength-toughness synergy in metastable austenitic stainless steel due to gradient structure formation. *Materials Letters*, 2021, vol. 303, p. 130585. DOI: 10.1016/j.matlet.2021.130585.
11. Huang M., Wang L., Yuan S., Wang J., Wang C., Mogucheva A., Xu W. Scale-up fabrication of gradient AGS in austenitic stainless steels achieves a simultaneous increase in strength and toughness. *Materials Science and Engineering: A*, 2022, vol. 853, p. 143763. DOI: 10.1016/j.msea.2022.143763.
12. Zhang J., Han W., Huang Z., Li J., Zhang M., Zhang L. Study on microstructure evolution and nanoindentation characteristics of 316 L austenitic stainless steel with inverse gradient grain sizes fabricated via torsion and electro-magnetic induction heating. *Materials Characterization*, 2021, vol. 181, p. 111462. DOI: 10.1016/j.matchar.2021.111462.
13. Wang H.T., Tao N.R., Lu K. Architected surface layer with a gradient nanotwinned structure in a Fe-Mn austenitic steel. *Scripta Materialia*, 2013, vol. 68 (1), pp. 22–27. DOI: 10.1016/j.scriptamat.2012.05.041.
14. Ho H.S., Zhou W.L., Li Y., Liu K.K., Zhang E. Low-cycle fatigue behavior of austenitic stainless steels with gradient structured surface layer. *International Journal of Fatigue*, 2020, vol. 134, p. 105481. DOI: 10.1016/j.ijfatigue.2020.105481.
15. Panov D.O., Kudryavtsev E.A., Chernichenko R.S., Naumov S.V., Klimenko D.N., Stepanov N.D., Zharebtsov S.V., Salishchev G.A., Sanin V.V., Pertsev A.S. Excellent strength-ductility combination of interstitial non-equiatomic middle-entropy alloy subjected to cold rotary swaging and post-deformation annealing. *Materials Science and Engineering: A*, 2024, vol. 898, p. 146121. DOI: 10.1016/j.msea.2024.146121.
16. Wu X., Zhu Y. Heterogeneous materials: a new class of materials with unprecedented mechanical properties. *Materials Research Letters*, 2017, vol. 5 (8), pp. 527–532. DOI: 10.1080/21663831.2017.1343208.



17. Wu X., Yang M., Yuan F., Wu G., Wei Y., Huang X., Zhu Y. Heterogeneous lamella structure unites ultrafine-grain strength with coarse-grain ductility. *Proceedings of the National Academy of Sciences of the United States of America*, 2015, vol. 112 (47), pp. 14501–14505. DOI: 10.1073/pnas.1517193112.
18. Chen A., Liu J., Wang H., Lu J., Wang Y.M. Gradient twinned 304 stainless steels for high strength and high ductility. *Materials Science and Engineering: A*, 2016, vol. 667, pp. 179–188. DOI: 10.1016/j.msea.2016.04.070.
19. Nayzabekov A., Lezhnev S., Maksimkin O., Tsai K., Panin E., Arbutov A. Microstructure and mechanical properties of austenitic stainless steel AISI-321 after radial shear rolling. *Journal of Chemical Technology and Metallurgy*, 2018, vol. 53 (3), pp. 606–611.
20. Panov D., Kudryavtsev E., Naumov S., Klimenko D., Chernichenko R., Mirontsov V., Stepanov N., Zherebtsov S., Salishchev G., Pertsev A. Gradient microstructure and texture formation in a metastable austenitic stainless steel during cold rotary swaging. *Materials*, 2023, vol. 16 (4), p. 1706. DOI: 10.3390/ma16041706.
21. Panov D., Chernichenko R., Kudryavtsev E., Klimenko D., Naumov S., Pertsev A. Effect of cold swaging on the bulk gradient structure formation and mechanical properties of a 316-type austenitic stainless steel. *Materials*, 2022, vol. 15 (7), p. 2468. DOI: 10.3390/ma15072468.
22. Chernichenko R.S., Panov D.O., Naumov S.V., Kudryavtsev E.A., Mirontsov V.V., Salishchev G.A., Pertsev A.S. Evolution of the structure, texture, and mechanical properties of austenitic stainless steel during annealing after cold radial forging. *Physics of Metals and Metallography*, 2023, vol. 124 (6), pp. 607–615. DOI: 10.1134/S0031918X23600537.
23. Yang M., Pan Y., Yuan F., Zhu Y., Wu X. Back stress strengthening and strain hardening in gradient structure. *Materials Research Letters*, 2016, vol. 4 (3), pp. 145–151. DOI: 10.1080/21663831.2016.1153004.
24. Beyerlein I.J., Tóth L.S. Texture evolution in equal-channel angular extrusion. *Progress in Materials Science*, 2009, vol. 54 (4), pp. 427–510. DOI: 10.1016/j.pmatsci.2009.01.001.
25. Suwas S., Ray R.K. *Crystallographic texture of materials*. London, Springer, 2014. 265 p. ISBN 978-1-4471-6313-8. DOI: 10.1007/978-1-4471-6314-5.
26. Fonda R.W., Knipling K.E. Texture development in friction stir welds. *Science and Technology of Welding & Joining*, 2011, vol. 16 (4), pp. 288–294. DOI: 10.1179/1362171811Y.0000000010.
27. Nesterenko V.F., Meyers M.A., LaSalvia J.C., Bondar M.P., Chen Y.J., Lukyanov Y.L. Shear localization and recrystallization in high-strain, high-strain-rate deformation of tantalum. *Materials Science and Engineering: A*, 1997, vol. 229 (1–2), pp. 23–41. DOI: 10.1016/S0921-5093(96)10847-9.
28. Chen Y., Liu G.M., Li H.Y., Zhang X.M., Ding H. Microstructure, strain hardening behavior, segregation and corrosion resistance of an electron beam welded thick high-Mn TWIP steel plate. *Journal of Materials Research and Technology*, 2023, vol. 25, pp. 1105–1114. DOI: 10.1016/j.jmrt.2023.06.010.
29. Hall E.O. The deformation and ageing of mild steel: II Characteristics of the Lüders deformation. *Proceedings of the Physical Society. Section B*, 1951, vol. 64 (9), pp. 742–747. DOI: 10.1088/0370-1301/64/9/302.
30. Petch N.J. The ductile-brittle transition in the fracture of  $\alpha$ -iron: I. *Philosophical Magazine*, 1958, vol. 3 (34), pp. 1089–1097. DOI: 10.1080/14786435808237038.
31. Abramova M.M., Enikeev N.A., Valiev R.Z., Etienne A., Radiguet B., Ivanisenko Y., Sauvage X. Grain boundary segregation induced strengthening of an ultrafine-grained austenitic stainless steel. *Materials Letters*, 2014, vol. 136, pp. 349–352. DOI: 10.1016/j.matlet.2014.07.188.
32. Humphreys F.J., Hatherly M. *Recrystallization and related annealing phenomena*. Elsevier, 2012. 520 p. ISBN 0080418848.
33. Wu X., Jiang P., Chen L., Yuan F., Zhu Y.T. Extraordinary strain hardening by gradient structure. *Proceedings of the National Academy of Sciences of the United States of America*, 2014, vol. 111 (20), pp. 7197–7201. DOI: 10.1073/pnas.1324069111.
34. Gao H., Huang Y., Nix W.D., Hutchinson J.W. Mechanism-based strain gradient plasticity – I. Theory. *Journal of the Mechanics and Physics of Solids*, 1999, vol. 47 (6), pp. 1239–1263. DOI: 10.1016/S0022-5096(98)00103-3.
35. Wilson D.V., Bate P.S. Influences of cell walls and grain boundaries on transient responses of an if steel to changes in strain path. *Acta Metallurgica et Materialia*, 1994, vol. 42 (4), pp. 1099–1111. DOI: 10.1016/0956-7151(94)90127-9.

## Conflicts of Interest

The authors declare no conflict of interest.